JOURNAL OF GEOPHYSICAL RESEARCH, VOL. 100, NO. B3, PAGES 3733–3745, MARCH 10, 1995

Mantle temperature anomalies along the past and paleoaxes of the Galápagos spreading center as inferred from gravity analyses

Garrett T. Ito[1] and Jian Lin

Department of Geology and Geophysics, Woods Hole Oceanographic Institution, Woods Hole, Massachusetts

Abstract. To better understand the effects of hot spots on mid-ocean ridge thermal structure, we investigate the subsurface density structure of the Galápagos spreading center and nearby lithosphere. Using shipboard gravity and bathymetry data, we obtain maps of mantle Bouguer anomalies (MBA) by removing from the free-air gravity the attractions of seafloor topography and a 6-km-thick model crust. Comparison of observed and theoretical MBA profiles along isochrons for ages 0.0-7.7 Ma suggests that seafloor topography is isostatically compensated by mass anomalies primarily in the upper 100 km of the mantle. This result is consistent with the notion that seafloor topography along the Galápagos spreading center is supported by lateral changes of crustal thickness and upper mantle density, both of which are controlled by temperatures in the upper mantle where decompression melting occurs. Along the ridge axis, the MBA decreases from the east and west toward the Galápagos hot spot by ~90 mGal, reaching a minimum nearest the hot spot at 91°W. Seafloor topography mirrors the MBA along axis, increasing by ~1.1 km toward the hot spot. These variations in MBA and bathymetry can be explained by crustal thickening and mantle density variations resulting from a gradual axial temperature increase of 50±25°C toward the hot spot. The predicted crustal thickening of 2-4 km nearest the hot spot accounts for 70-75% of the along-axis MBA and bathymetry anomalies; mantle density variations account for the rest of the anomalies. From the crustal isochron of age 7.7 Ma to the present-day axis, the along-isochron amplitudes of MBA decrease from ~150 to ~90 mGal. The corresponding along-isochron bathymetry anomalies decrease from ~1.7 to ~1.1 km. These observations along the paleoaxes of the Galápagos spreading center indicate that the axial temperature anomaly was 70% hotter in the past (86±25°C) and has steadily decreased to 50±25°C as the ridge axis migrated away from the Galápagos hot spot. These along-isochron temperature anomalies, however, have remained well below that estimated for the hot spot itself (200°C), indicating that the lateral temperature gradient between the hot spot and the ridge axis has remained 10-20 times greater than that along the ridge axis over the past 7.7 m.y.

Introduction

Three-dimensional gravity studies of mid-ocean spreading centers have proven crucial to understanding the processes controlling oceanic lithosphere accretion. For example, it has been shown that gravity and seafloor depth vary systematically along individual spreading segments [e.g., *Kuo and Forsyth,* 1988; *Prince and Forsyth*, 1988; *Lin et al.*, 1990; *Detrick et al.,* 1995] and appear to be spreading-rate-dependent [*Parmentier and Phipps Morgan*, 1990; *Lin and Phipps Morgan*, 1992; *Sparks et al.,* 1993]. Such variations in gravity and bathymetry indicate segment-scale changes in crustal thickness and/or mantle density and thus may reflect anomalies in along-axis mantle temperatures. Near hot spots, however, the extent of along-axis variation in density structure is broader than individual ridge segments, indicating a larger scale influence by mantle plumes [*Anderson et al.*, 1973; *Cochran and Talwani,* 1977; *Bell and Buck,* 1992]. The influence of mantle plumes on crustal composition is also evident by enrichments of trace elements and isotopes along the Reykjanes Ridge near the Iceland hot spot [*Hart et al.*, 1973; *Schilling,* 1973, 1975a; *Vink*, 1984], along the Mid-Atlantic Ridge near the Azores hot spot [*White et al.*, 1975, 1976; *Schilling*, 1975b], and along the Galápagos spreading center near the Galápagos hot spot [*Schilling et al.*, 1976, 1982; *Verma and Schilling*, 1982; *Verma et al.*, 1983].

The Galápagos spreading center is an excellent example of an oceanic ridge influenced by a nearby hot spot. At present-day, the spreading center lies ~170 km north of the Galápagos hot spot and separates the Cocos Plate to the north and the Nazca Plate to the south with a full spreading rate of 4.5-6.8 cm/yr [*DeMets et al.,* 1990] (Plate 1a). Spreading segments of the Galápagos spreading center trend east-west and are adjoined by north-south trending transform faults. *Hey* [1977] proposed that the Galápagos hot spot began forming the Cocos and Carnegie Ridges ~20 Ma and then migrated southwest with respect to the Cocos Plate as it continued accreting the Cocos Ridge. The spreading center crossed over the hot spot 5-10 Ma as the Galápagos Archipelago began its formation on the Nazca Plate.

As for the present-day interaction between the hot spot plume and spreading center, it was first suggested by *Morgan* [1978]

[1]Also at MIT/WHOI Joint Program in Oceanography, Woods Hole Oceanographic Insitution, Woods Hole.

Paper number 94JB02594.
0148-0227/95/94JB-02594$05.00

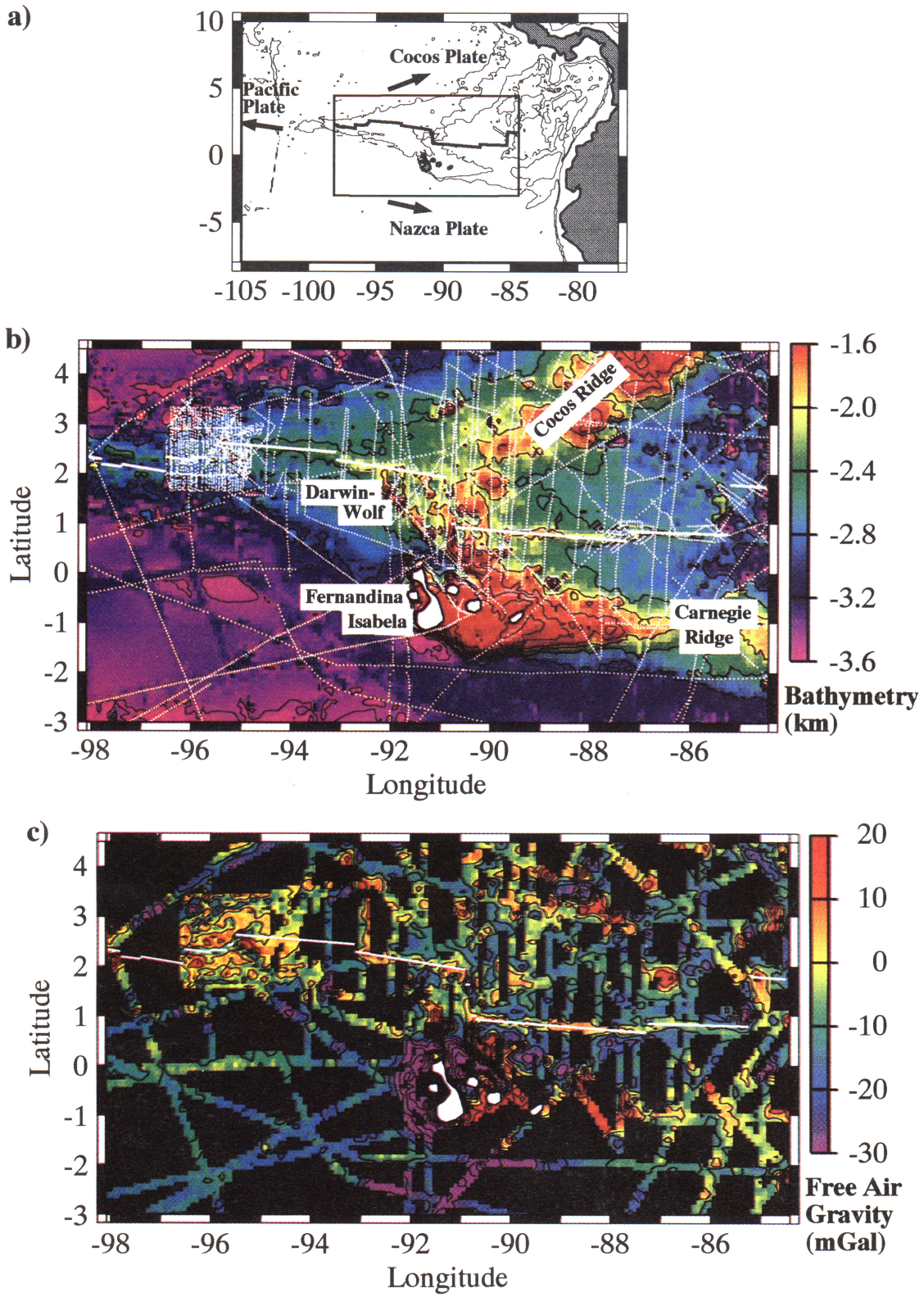

Plate 1. (a) Tectonic map of the Galápagos spreading system encompassing the study region (rectangular box). The solid dark lines mark the ridge axis, and the arrows show the estimated absolute plate motion relative to the hot spot reference frame. (b) Color-shaded map of shipboard and DBDB5 bathymetry illuminated from the north and contoured at 500-m intervals. Depths shallower than 1.6 km are colored red, while those deeper than 3.6 km are colored violet. Grid spacing is 5-min. The spreading center is marked by solid white lines and the gravity ship tracks are marked by white dotted lines. (c) Color map of free-air gravity along ship tracks with contour interval of 10 mGal and gridded with 5-min spacing. Gravity values >20 mGal are colored red, while those <-30 mGal are colored violet. The contours are drawn from interpolated values between ship tracks and are masked in regions with no data.

that Galápagos plume material feeds through a mantle conduit into the Galápagos spreading center giving rise to the Wolf-Darwin seamount chain (Plate 1b). Plume-fed mantle flow along axis was suggested by *Vogt* [1976] to explain the uniform increase in along-axis topography toward the hot spot. Further evidence for plume flow toward and along the spreading center is rare earth enrichments along the ridge, first documented by *Schilling et al.* [1976]. Subsequent studies of along-axis variation in rare earth element and isotopic ratios support ideas of plume entrainment to the ridge axis and along-axis dispersion of plume material [*Verma and Schilling*, 1982; *Verma et al.*, 1983; *Schilling*, 1985].

In this paper we present evidence for a regional mantle temperature anomaly and an associated crustal thickness variation beneath the Galápagos spreading center imposed by the Galápagos hot spot. We first isolate the subsurface component of the gravity field by making topographic and crust-mantle interface corrections (the mantle Bouguer corrections). We next examine topographic compensation mechanisms both on- and off-axis by comparing theoretical and observed mantle Bouguer gravity anomalies along isochrons for models of compensation from crustal thickness variations (Airy compensation) and compensation from laterally varying mantle densities (Pratt compensation). Given the constraints on the depth of compensation, we then examine models of crustal and mantle density structure to constrain mantle temperatures along the present-day Galápagos spreading center. Finally, we discuss the temporal evolution of axial mantle temperatures in the past 7.7 m.y. and its implications for the evolution of this hot spot-ridge system.

Data

Our approach for investigating mantle temperature anomalies requires accurate constraints on subsurface density structure which is reflected directly by gravity and seafloor topography. The gravity and bathymetry data we use are shipboard data obtained from the National Geophysical Data Center and the Lamont-Doherty Earth Observatory. The data set covers a region within 84.4°-98.1°W and 3.0°S-4.5°N, encompassing the Galápagos spreading center and the Galápagos hot spot (Plate 1b). We also use high-resolution gravity and bathymetry data from a dense survey around the 95.5°W propagating rift tip [*Phipps Morgan and Kleinrock*, 1991]. The bathymetry data are shipboard depth soundings supplemented with digital bathymetry (DBDB5) between ship tracks. DBDB5 data points within 5 min of a ship data point are eliminated and the combined data set is regridded with 5-min grid spacing to produce the bathymetry map shown in Plate 1b. A regional bathymetric swell encompassing the Galápagos Archipelago spans ~1300 km along the ridge axis. The swell shallows along the ridge axis toward 91°W by 1.1 km and peaks near the Galápagos hot spot which is centered beneath the island Fernandina [*White et al.*, 1993] (see Figure 1b for along-axis profile).

In order to improve the internal consistency of the gravity data we use the method of *Prince and Forsyth* [1984] to minimize discrepancies in gravity measurements at ship track crossings. Applying the appropriate DC shifts to straight-line track segments reduces the total rms crossover error from 11.2 to 5.5 mGal. The value of 5.5 mGal is therefore our estimate for data uncertainty. After applying these corrections we produce the 5-min grid of free-air gravity shown in Plate 1c. In this map we observe short-wavelength (<100 km) peaks coinciding with topographic highs; the lowest free-air gravity (-90 mGal) occurs over the flexural moat of the Galápagos Archipelago and the highest (+60 mGal) occurs over the southeastern flank of the island of Isabela (see Plate 1b for location of Isabela). The total variation in free-air gravity along the ridge axis is ~40 mGal.

We use only shipboard gravity rather than satellite-altimetry-derived gravity because the released satellite data coverage in this region is still sparse and the shipboard gravity is more accurate. The other reason for using only shipboard gravity concerns the accuracy of topographic corrections which rely on accurate bathymetric measurements. Since shipboard gravity and bathymetric measurements are taken at the same points, topographic corrections to the free-air gravity are the most accurate possible.

Gravity Data Reduction

A significant portion of the free-air gravity is caused by seafloor topography. Therefore, to investigate subsurface density structure, to which we will relate mantle temperature anomalies, we apply a mantle Bouguer correction. Using Parker's [1973] spectral method, we subtract from the free-air gravity the theoretical gravity signal of the seafloor-water interface and crust-mantle (Moho) interface assuming a crustal layer of constant thickness (6 km) and density (2800 kg/m^3). We take the density of the mantle to be 3300 kg/m^3.

The resulting mantle Bouguer anomaly (MBA) shows that most of the short-wavelength (<100 km) variations caused by local topography are removed, leaving a broad oval-shaped negative anomaly aligned along the spreading axis between ~97°W and ~85°W (outlined by yellow shading, Plate 2a). Superimposed on this oval-shaped anomaly are high-amplitude negative branches over the Cocos Ridge (<-100 mGal) and Galápagos Archipelago (<-300 mGal) reflecting the thickened crust of these edifices. Along the ridge axis, 10-20 mGal variations in MBA occur at segmentation length scales (100-200 km), but the most prominent feature is the long-wavelength decrease by ~90 mGal along axis toward 91°W (Plate 2b). For comparison with other oceanic spreading centers, this 90-mGal anomaly is approximately twice the segmentation-scale MBA variation along the Mid-Atlantic Ridge [e.g., *Lin et al.*, 1990; *Detrick et al.*, 1995] and about 10 times the MBA variation along the East Pacific Rise (8.8°-13.5°N) [*Madsen et al.*, 1990].

The minimum in MBA occurs near 91°W on the southern segment of the 91°W-transform offset, which is also the point of the ridge axis closest to the Galápagos hot spot (point P, Plate 2a). The decrease in MBA is nearly symmetric about point P and uniform along the 650-km ridge length to each side of point P. This wavelength is comparable in extent to topographic swells of other hot spots such as Hawaii (~1500 km across the island chain), Cape Verde (~1500 km in diameter) [*Crough*, 1983], and Iceland (~2000 km in diameter) [*White*, 1988].

Comparison of this along-axis MBA with along-axis variations in bathymetry and basalt chemistry reveals a close correlation between the four anomalies (Figure 1). All anomalies peak at or near point P, all extend over comparable length scales, and all decrease in amplitude nearly symmetrically eastward and westward away from point P. The peak in the La/Sm anomaly coincides with that of K_2O, MgO, and a minimum in FeO [*Schilling et al.*, 1982], while the peak in $^{87}Sr/^{86}Sr$ coincides with a minimum in $^{143}Nd/^{144}Nd$ [*Verma et al.*, 1983]. Both geochemical signatures are attributed to a source heterogeneity associated with the Galápagos hot spot [*Verma et al.*, 1983]. Although the peak in $^{87}Sr/^{86}Sr$ occurs ~100 km west of point P, this offset is small relative to the total wavelength of the above

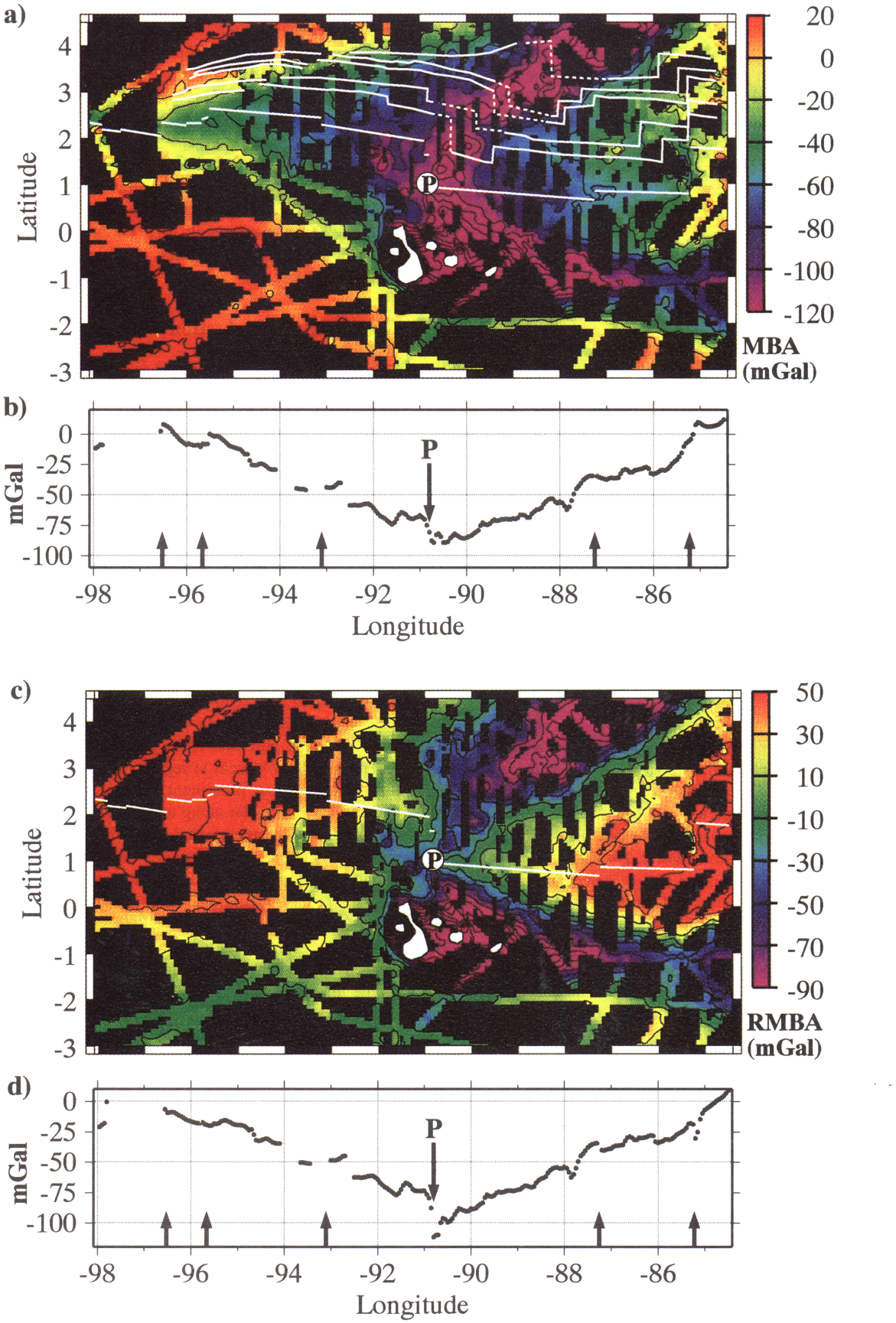
a)
Latitude
4
3
2
1
0
-1
-2
-3
P
20
0
-20
-40
-60
-80
-100
-120
MBA
(mGal)
b)
mGal
0
-25
-50
-75
-100
P
-98
-96
-94
-92
-90
-88
-86
Longitude
c)
Latitude
4
3
2
1
0
-1
-2
-3
P
50
30
10
-10
-30
-50
-70
-90
RMBA
(mGal)
d)
mGal
0
-25
-50
-75
-100
P
-98
-96
-94
-92
-90
-88
-86
Longitude

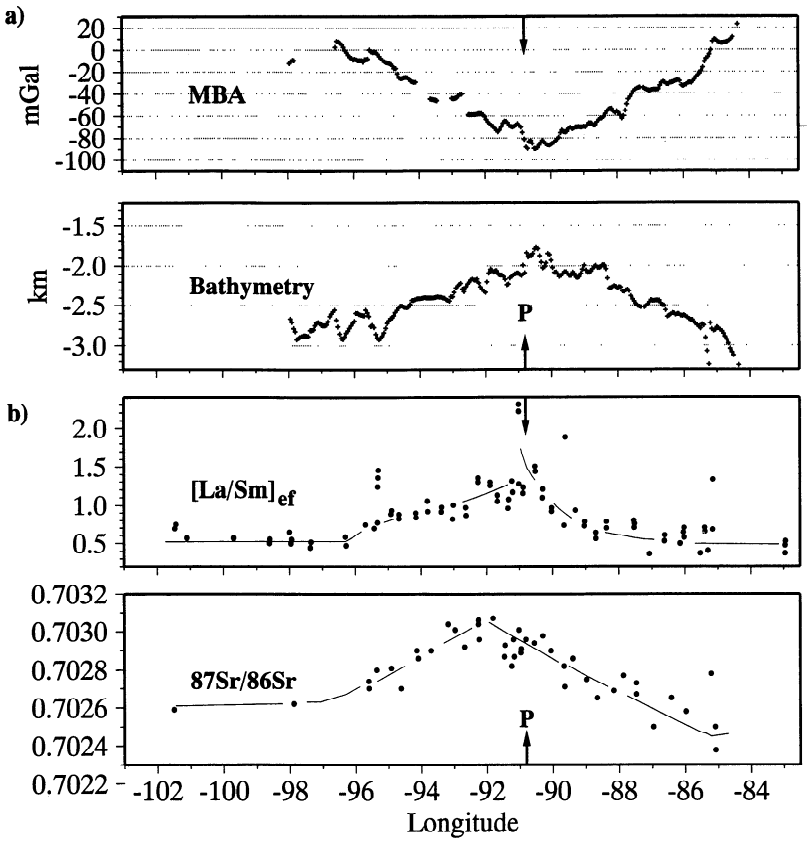

Figure 1. (a) Along-axis mantle Bouguer (MBA) and bathymetry profiles are compared with along-axis variations (b) in $[La/Sm]_{ef}$ and $^{87}Sr/^{86}Sr$ [*Verma et al.*, 1983]. Note that the peaks for all anomalies except for $^{87}Sr/^{86}Sr$ coincide at point P.

anomalies and within the 150 to 300-km diameter suggested for intraplate hot spots [*Epp*, 1984; *McNutt*, 1989]. The correlation of MBA and bathymetry with basalt chemistry suggests that the along-axis density structure is closely related to the enriched material introduced by Galápagos plume beneath the ridge axis.

The final step in our gravity analysis is to remove the predictable effects due to lithospheric cooling. Calculation of the three-dimensional (3-D) distribution of temperature-dependent mantle densities for passive mantle upwelling is relatively simple using a standard method first presented by *Phipps Morgan and Forsyth* [1988]. We use a spectral method to solve for flow of a constant-viscosity mantle, driven by two spreading plates with the geometry of the Galápagos spreading center. Using finite difference approximations for the conductive-advective heat balance equation, we solve for steady state mantle temperatures, from which we derive mantle densities assuming a thermal expansion coefficient of 3.4×10^{-5} °C^{-1}. The integrated gravity fields from each density layer down to a 100-km depth represent the lithospheric cooling contribution to the gravity field [*Kuo and Forsyth*, 1988].

We subtract the lithospheric cooling effects from the MBA to produce the residual mantle Bouguer gravity anomaly (RMBA), shown in Plate 2c. The oval-shaped MBA low, observed between ~97°W and ~85°W, is removed by the lithospheric cooling correction; what remain are high-amplitude negative anomalies branching from the ridge axis, over the Galápagos Archipelago and the Cocos and Carnegie Ridges. These negative RMBA branches reflect the anomalous volcanic and mantle density

Plate 2. (a) Contour and color-shaded map of the mantle Bouguer anomaly. Anomaly values >20 mGal are colored red, while those <-120 mGal are colored violet. Interpolated values between ship tracks are masked, and the spreading center and islands are marked in white. Note the oval-shaped negative anomaly aligned along the spreading center between ~97°W and ~85°W (outlined by the yellow shading) and the negative anomaly branches of the Cocos Ridge and Galápagos Archipelago. The five white profiles north of the spreading center mark isochrons from *Wilson and Hey* [1995] used for the off-axis analysis. Profiles are dashed in regions where magnetic lineations are extrapolated. (b) Mantle Bouguer gravity values extracted along the spreading center. Note that the anomalies reach a minimum at point P, where the ridge axis is closest to the hot spot. The arrows mark locations of transform offsets. (c) Map of residual mantle Bouguer anomaly with contour interval of 20 mGal and a color range of -90 to +50 mGal. Note high-amplitude negative anomalies along the Cocos Ridge, the Darwin-Wolf seamounts, and the Galápagos Islands (shown in white). (d) Along-axis profile of residual mantle Bouguer anomaly showing ~100 mGal decrease from the east and west toward point P. Arrows mark transform offsets.

structure left along the Galapágos hot spot tracks. The dominant effect of the lithospheric correction on the along-axis profiles is to reduce the segment-scale variations in the MBA; it does not appreciably affect the long-wavelength decrease due to the hot spot (Plate 2d). Although the amplitude of the along-axis RMBA is increased slightly (by 10 mGal) from that of the along-axis MBA, the lateral extent and location of the maximum are the same for the two anomalies. For this reason, we focus on the MBA for the remainder of the paper.

Compensation of Topography

The mantle Bouguer correction has been widely used as a first-order correction for oceanic crustal structure [e.g. *Kuo and Forsyth*, 1988; *Lin et al.*, 1990; *Madsen et al.*, 1990; *Blackman and Forsyth*, 1991; *Morris and Detrick*, 1991] since the total global variation in oceanic crustal thickness is ~3 km about a mean of 6 km [*Chen*, 1992]. Our assumption of a constant 6-km-thick crust is merely a first approximation of crustal structure from which we reference departures in density structure. Deviations from this reference model could be lateral variations in crustal thickness, lateral mantle density variations, or a combination of the two. The nonuniqueness of gravity solutions necessitates additional constraints. An obvious constraint is topography since, if in isostatic equilibrium, it too depends directly on density structure. Here we test two modes of isostatic compensation: (1) crustal compensation (Airy isostasy) and (2) compensation from lateral density variations in the mantle (Pratt isostasy).

Airy and Pratt Isostasy Admittance Functions

The theoretical mantle Bouguer gravity anomaly due to the two modes of isostatic compensation is solved using standard spectral methods as follows. In the spectral domain, the mantle Bouguer gravity anomaly $B(\mathbf{k})$ is related to bathymetry $H(\mathbf{k})$ by an isostatic response function, or admittance function $Q(k)$, according to

$$B(\mathbf{k})=Q(k)\cdot H(\mathbf{k}) \qquad (1)$$

where $\mathbf{k}$ is the two-dimensional wavenumber, $k=|\mathbf{k}|=2\pi/\lambda$. Included in $Q(k)$, are the effects of density structure that differs from the "reference" structure (i.e., a crust of uniform thickness overlying a mantle of uniform density). In Airy compensation models, it is the crustal structure that differs from the "reference" since topography is assumed to be supported by laterally varying crustal thickness. If we assume that elevated topography is supported by crust that is anomalously thick, the admittance function must include two terms to account for the effects at two interfaces as follows:

$$Q(k)=-2\pi G[\Delta\rho\exp(-kz_c)+\rho_c\exp(-kz_o)], \qquad (2)$$

where $G=6.67\times10^{-11}$ m^3/kg s^2 is Newton's gravitational constant, $\Delta\rho$ is the crust-mantle density contrast (500 kg/m^3), and ρ_c is the crust-water density contrast (1800 kg/m^3). The first term replaces the attraction of mantle by that of crust at the "reference" Moho (z_c=8.7 is the average seafloor depth of 2.7 km plus 6.0 km). The second term accounts for the effects of the Airy crustal root at its assumed mean depth z_o of 11.0 km beneath the sea surface.

For Pratt compensation, it is mantle density that differs from the "reference" structure since topography is assumed to be compensated by laterally varying mantle densities. The amplitude of the density reduction in a vertical column required to support a given topographic elevation is $H\rho_m/z_p$ where ρ_m is the mantle-water density contrast (2300 kg/m^3) and z_p is the depth of compensation. The Pratt admittance function must therefore consider the integrated effects of all density layers from z_c to (z_c+z_p) and is thus defined as

$$Q(k)=-2\pi G\rho_m\exp(-kz_c)\frac{[1-\exp(-kz_p)]}{kz_p}. \qquad (3)$$

Results

Mantle Bouguer profiles taken along the present-day ridge axis and selected isochrons (Plate 2a) are compared with the Airy and Pratt theoretical profiles (Figure 2a). The standard deviation misfit between theoretical and observed profiles is plotted versus

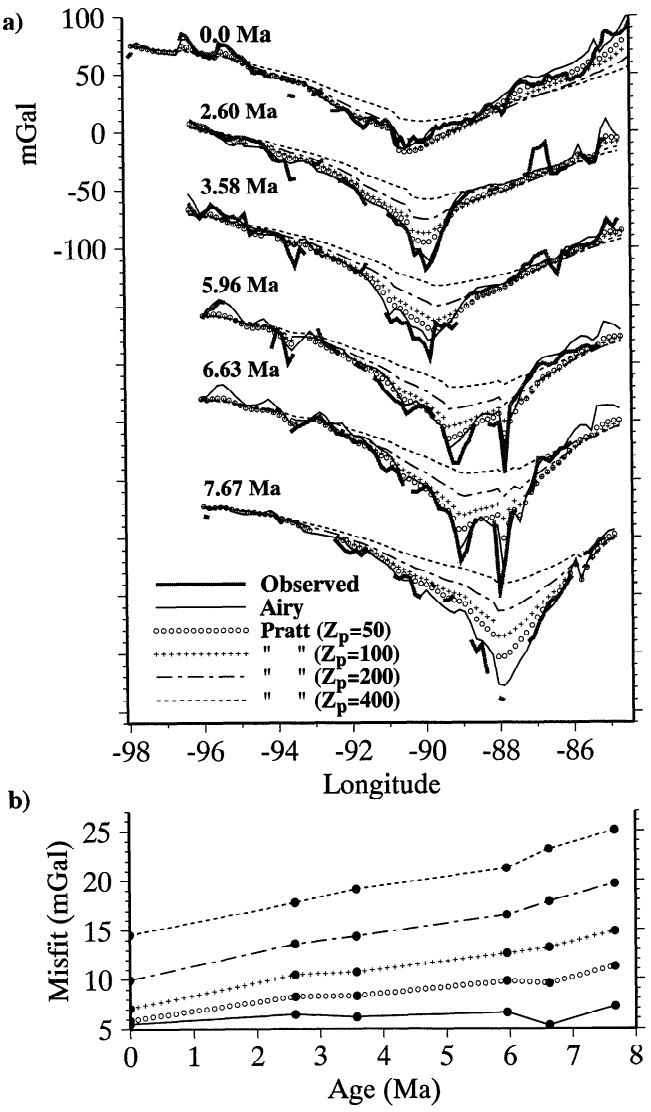

Figure 2. (a) Profiles of observed mantle Bouguer anomalies (shaded profiles) are compared with theoretical models for different assumed compensation mechanisms and depths. The locations of the off-axis crustal isochrons (labeled with ages from *Wilson* [1993]) are in Plate 2c. (b) The standard deviation misfit is plotted against crustal age for the five compensation models tested. Note that models of shallow depths of compensation yield the smaller misfits.

age in Figure 2b. For the crustal ages examined (0.0-7.67 Ma) the standard deviation misfit for the Airy compensation profiles has a nearly constant value of ~6 mGal, which is close to our estimated data uncertainty of 5.5 mGal. For the Pratt compensation models, standard deviation misfits increase with compensation depth (z_p) and with age. Along the present-day axis, the Pratt models of z_p=50 and 100 km are the most reasonable with standard deviations of 5.9 and 7.1 mGal, respectively.

Although the Airy profiles yield the lowest misfits to the observed MBA, the Pratt calculations with shallow compensation depths (z_p=50 and 100 km) also yield small misfits. Most of the misfit by the shallow Pratt calculations appears to be due to short-wavelength variations (<200 km) in the observed MBA which may come from local variations in crustal structure. We thus do not exclude the possibility that at least some of the gravity and topographic signal is due to density variations in the shallow mantle. The increase in misfits with age for the Pratt calculations may, however, reflect a decrease in the mantle contribution relative to that of the crust along paleoridge axes.

Topography may also be supported dynamically by lithospheric or upper mantle stresses. Previous work has shown that shallow stresses induced by plate spreading contribute significantly to axial topography [e.g., *Phipps Morgan et al.*, 1987; *Lin and Parmentier,* 1989; *Small and Sandwell*, 1989; *Chen and Morgan*, 1990; *Neumann and Forsyth*, 1993]. *Neumann and Forsyth* [1993], for example, demonstrated that the correlation between gravity and topography along the Mid-Atlantic Ridge is due to dynamic stresses in the lithosphere which depend on crustal thickness and mantle thermal structure. However, for the Galápagos spreading rates of 48-64 mm/yr and possible crustal thickness structure, these extension-related stresses would be small [*Neumann and Forsyth*, 1993]. Significant topography (>1 km) can also be maintained by viscous stresses in a convecting mantle [*Anderson et al.*, 1973; *McKenzie et al.,* 1980]. If viscous stresses are important along the Galápagos spreading center, they must be associated with low densities in the shallow mantle as indicated by our MBA modeling (Figure 2). We thus suggest that the long-wavelength topography of the Galápagos spreading center and nearby Cocos Plate is essentially isostatic and is supported by density anomalies primarily within 100 km beneath the seafloor.

Present-Day Axial Mantle Temperatures

As demonstrated above, crustal thickness and shallow mantle density variations are both likely sources of topographic compensation. We suggest that they both occur and that both are controlled by mantle temperature: crustal thickness by temperature-enhanced melting, and mantle density by thermal expansion. For the following analysis, we investigate the mantle temperature variation required to generate the ~90-mGal variation in along-axis MBA and the ~1.1-km increase in axial topography.

Model Configuration

Using the same numerical methods as were used for the lithospheric cooling calculations, we solve for 3-D mantle temperatures due to passive upwelling; this time, however, we impose a temperature anomaly ΔT at the base layer (Figure 3). To estimate the additional crust that may result from a given ΔT, we take the fraction of partial melting f to depend on mantle temperature T by $f=(T-T_s)/600°$, where T_s is the mantle solidus

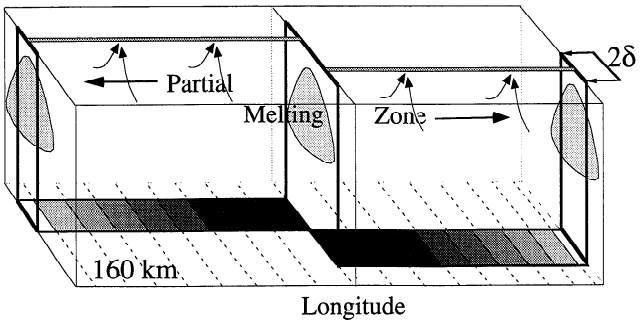

Figure 3. Schematic illustration of our simplified 3-D melt generation models. The ridge axis (shaded gray lines at the top surface) is offset by the 91° transform fault. The region of melt transport, with width 2δ, is outlined by the bold dark lines. The melting zone beneath ridge segments is shown on depth cross sections as shaded triangular shapes; curved arrows denote melt transport toward the ridge axis. The region of melt transport at the base layer is shaded gray according to the imposed temperature with the greatest temperature anomaly near the 91° transform fault.

and 600°C is the supersolidus temperature required to fully melt a unit volume of peridotite [*Reid and Jackson*, 1981]. The rate of melt generation $\dot{f}$ depends on the gradient of f and mantle flow rate $\mathbf{v}$ by $\dot{f}=\mathbf{v}\cdot\nabla f$ [*Reid and Jackson*, 1981]. We estimate the mantle solidus to be linearly dependent on pressure and thus depth z (in kilometers below the seafloor), by T_s=1100°C + 3.25(°C/km)z. Crustal accretion at the ridge crest depends on the spatial distribution of melting and subsequent migration of melt toward the ridge. The process of melt migration is still largely unconstrained; therefore we simplify this calculation by treating ridge segments as line sinks which draw in melt from the mantle below [*Phipps Morgan and Forsyth*, 1988]. Assuming that melt migrates over a finite lateral extent, we define a width δ, on each side of the ridge axis, as the region of melt transport (Figure 3); outside of this melt transportation zone, we assume that melts are carried away by the cooling lithospheric plates thus do not contribute to the crust. We also assume that a small melt fraction f_o is retained in the mantle matrix within this zone of melt transport. We adjust the parameters δ and f_o such that the resulting crustal thickness for a normal base layer temperature (1350°C) is 6 km at the ridge segment centers. This result is achieved for f_o values of 0-6% [*Forsyth*, 1992] and corresponding δ values of 30-50 km. We assume that f_o does not vary along-axis therefore it does not contribute to the long-wavelength variation in mantle density. The base layer is set to a depth of 160 km to ensure that the entire melting region is included.

Base Layer Temperature Distributions

For the base layer temperature anomalies, we investigate three geometries. In our first set of calculations (model A), we vary temperatures linearly along-axis with the maximum anomaly beneath the 91°W transform (Figure 4a). This is the simplest model, designed to test the effects of strictly along-axis variation in temperatures. For the second set of calculations (model B), we impose a circular anomaly centered on the island Fernandina, thought to mark the current location of the Galápagos hot spot center [*White et al.*, 1993] (point H, Figure 4b). Temperatures decrease linearly away from point H. We envision this model to represent the temperature distribution from a radial dispersion of plume material from the hot spot center. For the third set of

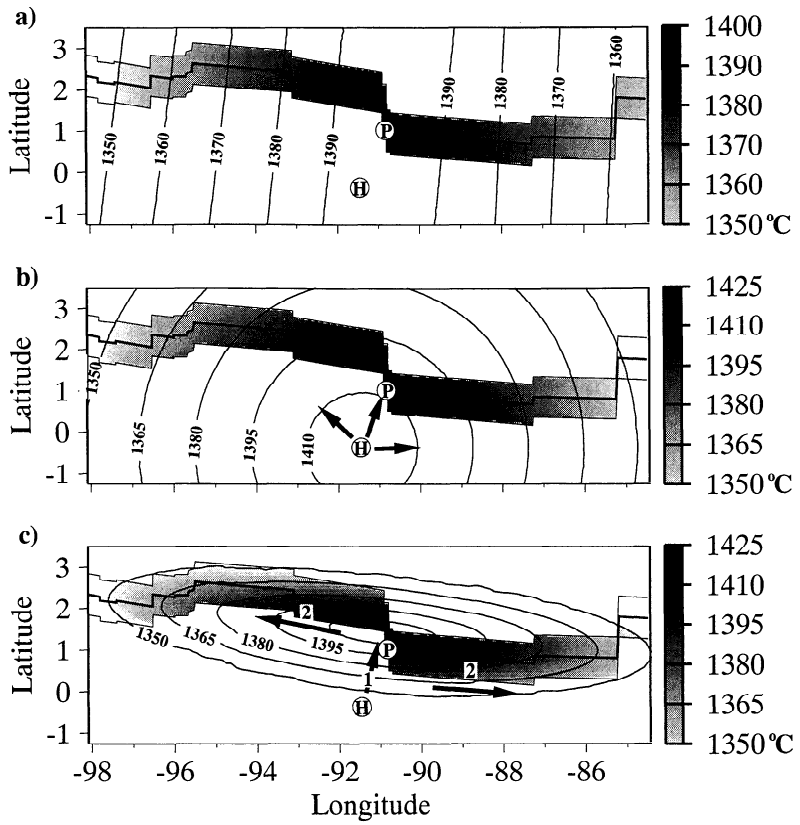

Figure 4. (a) Map of temperatures imposed at the base layer of our best fitting linear model A. Temperatures in the zone of melt transport are shaded to emphasize the importance of this region in gravity and bathymetry calculations. Point H marks the location of the Galápagos hot spot, while point P marks the location of the peak in along-axis MBA and bathymetry. (b) Temperatures imposed at the base layer of our best fitting circular model (model B) with maximum temperature located at point H. Arrows denote hypothetical radial dispersion of hot spot material from point H. (c) Base layer temperatures imposed for our best fitting elliptical model (model C). Arrows denote plume channeling from point H to point P (arrow 1) and then along-axis away from P (arrows 2).

calculations (model C), we use an elliptical temperature anomaly which is centered midway along the 91°W transform and decreases linearly away from the ellipse center (Figure 4c). This model is designed to approximate the temperature distribution along the ridge axis that might result from *Schilling's* [1985, 1991] plume flow model which incorporates ideas of *Vogt* [1976] and *Morgan* [1978]. According to this model, Galápagos plume material feeds through a conduit connecting point H to the ridge axis (arrow 1, Figure 4c), and then disperses preferentially along axis (2 arrows, Figure 4c). We approximate the preferential along-axis flow as an ellipse aligned with the ridge axis. Each of the three models has a base layer temperature maximum near point P directly beneath the ridge axis with a gradual decrease along axis toward the east and west edges of the study region. Gravity and bathymetry calculations for these models are sensitive mostly to temperature conditions within the region of melt transport since only melts in this region are assumed to contribute to accretion of the crust.

Results

Gravity calculations for the three models are done by applying *Parker's* [1973] method to the density layers in the mantle and the crust-mantle interface treating the crustal thickness as only varying along-axis. Since we have shown that the long-wavelength seafloor topography is compensated at shallow depths, we calculate theoretical bathymetry assuming Airy compensation for the crust and Pratt compensation for the mantle shallower than 160 km. Figures 5a and 5b compare theoretical results of model A for different base layer temperature anomalies at point P (ΔT_p) with observed MBA and bathymetry profiles. Profile sections near transform faults are omitted since our models gave unrealistically small crustal thicknesses due to local cooling effects near ridge segment ends. Removal of these local effects, however, do not affect the larger-scale thermal anomaly related to the Galápagos hot spot.

As illustrated in Figures 5a and 5b, the model for ΔT_p of 50°C best fits both the MBA and bathymetry profiles. The ΔT_p=25 and 75°C solutions are the upper and lower limits for model A. Table 1 outlines the corresponding results of models B and C and the associated standard deviation misfits. Despite differences in the detail 3-D temperature structure between the three models, all three suggest similar values of ΔT_p with comparable minimum misfit. This finding indicates that axial crustal and density structure is sensitive primarily to temperatures directly beneath the ridge axis and insensitive to subtle temperature changes away from the ridge axis. We conclude ΔT_p to be ~50±25°C with a corresponding crustal thickening of 3±1 km (Figure 5c). As the crust thickens toward point P, it gives rise to 70-75% of the topographic swell and MBA gravity signal. The remaining 25-30% of topography and gravity signal is supplied by the anomalously hot and less dense mantle beneath the ridge axis.

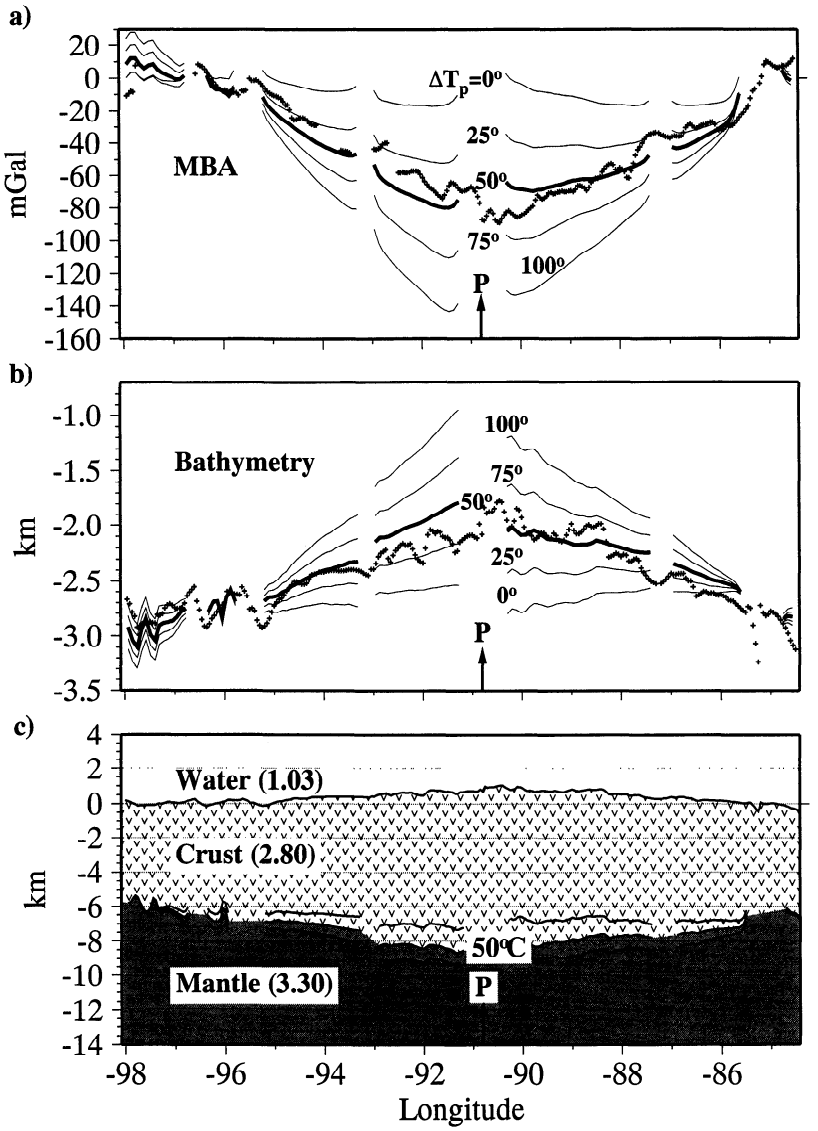

Figure 5. The observed profiles (small crosses) of (a) along-axis MBA and (b) bathymetry are compared with theoretical profiles from model A with different values of point P, base layer temperature anomalies, ΔT_p. Sections of profiles near transform faults are omitted to accentuate the broad wavelength anomaly (solid lines) associated with the hot spot. The best fitting profiles are denoted by bold lines. (c) Predicted along-axis cross section of the crustal structure based on model A results. The Moho is drawn according to our best fitting result (+50°C model); the two other profiles are drawn according to the +25°C (shallower curve) +75°C (deeper curve) results. The Moho boundary is omitted near transform faults as marked by arrows. Densities are in grams per cubic centimeter.

Our crustal model is consistent with estimates of *Feighner and Richards* [1994] based on flexural modeling of gravity near the Galápagos Archipelago. Confirming this crustal model, however, requires future marine seismic experiments since few seismic constraints exist to date.

Discussion

Our primary focus in this study is the effects of mantle temperature on crustal thickness and on mantle density changes by thermal expansion. A number of factors not incorporated into our models may also contribute to crustal thickness and mantle density structure and lead to changes in our ΔT_p estimate. These include (1) compositionally dependent and disequilibrium melting, (2) melt depletion and latent heat loss in the mantle, (3) buoyancy-driven mantle flow, and (4) mantle compositional effects on melting and on mantle densities. We briefly discuss these factors below.

Compositionally dependent and disequilibrium melting. The simple linear melt function and linear depth-solidus relation that we used was defined by *Reid and Jackson* [1981] based on results of batch melting experiments in which melt maintained equilibrium with the remaining solid phases. If melt is extracted rapidly in the mantle such that it fails to equilibrate with the matrix, then the solidus of the depleted residue increases with increasing melt extents [*Kinzler and Grove*, 1992; *Cordery and Phipps Morgan*, 1993]. If this disequilibrium melting scenario is the dominant process in the mantle, then a greater ΔT_p than we estimated may be required beneath the Galápagos spreading center to thicken the crust by 3±1 km.

Melt depletion and latent heat loss in the mantle. In addition to inhibiting melting, melt depletion may also reduce

Table 1. Model Results

	MBA		Bathymetry	
	Best Fit ΔT_p, °C	Misfit, mGal	Best Fit ΔT_p, °C	Misfit, km
Model A	50±25	9	50±25	0.13
Model B	49±25	10	49±25	0.13
Model C	47±25	8	49±25	0.14

mantle densities, primarily by decreasing the Fe/Mg ratio of the residue [*Oxburgh and Parmentier*, 1977]. The opposite effect, however, may result from latent heat removal which cools the mantle thus increases its density. Numerical experiments by *Magde et al.* [1995] indicate that to generate an oceanic crust of normal thickness, the two factors would lead to a net decrease in mantle densities of the order of 1%, or ~6 times the thermal expansion effect of heating the mantle by 50°C. This potential density reduction may contribute to the Galápagos bathymetry and gravity anomalies significantly enough that the crustal thickness and thus ΔT_p are smaller than we estimated.

Buoyancy-driven mantle flow. In addition to their direct signature on surface observables, mantle density variations lead to buoyancy forces which drive mantle flow. Beneath normal oceanic spreading centers the dominant sources of buoyancy are most likely melt depletion-related and melt retention-related density reductions [*Jha et al.*, 1994]. If buoyancy forces are important, they are likely to enhance vertical flow and increase the rate of melting and thus may lead to a lower ΔT_p prediction.

Mantle compositional effects on melting and on mantle densities. A hot spot-related temperature anomaly as investigated in this study is an obvious source for thickened crust and reduced mantle densities; however, mantle source heterogeneity may also play important roles. Enrichment in volatile [*Bonatti*, 1990] or incompatible elements [*Michael et al.*, 1994] in the mantle may enhance melting and thus yield a thicker crust for a given mantle temperature anomaly. While there is little evidence for a volatile enrichment beneath the Galápagos spreading center, there is evidence for an increase in incompatible element concentration toward point P from ridge axis samples [*Schilling et al.*, 1982; *Langmuir et al.*, 1992]. In addition, a decrease in Fe/Mg was observed in axial samples toward point P [*Schilling et al.*, 1982; *Langmuir et al.*, 1992], possibly reflecting a low Fe/Mg and thus low-density mantle source near the Galápagos hot spot. Including such heterogeneities of the mantle source in incompatible element content and Fe/Mg ratio may yield a lower ΔT_p estimate.

In summary, while considering factor 1 would increase an estimate of ΔT_p, considering factors 2, 3, and 4 would substantially decrease an estimate of ΔT_p. We therefore anticipate that our estimate of ΔT_p is an upper bound, although the interplay of the above four factors may be complex and requires comprehensive investigation that is beyond the scope of this study.

By considering the first-order aspects of mantle flow, heat transport, and decompression melting, we have established a relation between crustal thickness, temperature-dependent mantle density, and mantle temperature anomaly. Our approach is consistent with previous studies of intraplate hot spot anomalies. For example, *Crough* [1978], *Sleep* [1990], and *McNutt* [1987] constrained hot spot temperature anomalies based on mantle-density anomalies which they took to be strictly temperature dependent. *McKenzie* [1984] constrained hot spot anomalies based on estimates of crustal thickness assuming, as we do, that melting occurs under equilibrium conditions. Our relationship between ΔT and the mantle component of topography is essentially the same as *Sleep's* [1990], and our relationship between ΔT and crustal thickness is consistent with that of *McKenzie* [1984] (50-75°C for crustal thickening of 2-4 km).

Our constraints on ΔT beneath the Galápagos spreading center have implications for the nature of heat transport both along the ridge axis and from the hot spot to the ridge axis. Using *Feighner and Richard's* [1994] estimate for the volcanic thickness of the Galápagos Archipelago (15-20 km) and *McKenzie's* [1984] melting relationships, we estimate a temperature anomaly of ~200°C at the hot spot center (point H, Figure 6). This temperature estimate is similar to the 214°C anomaly estimated by *Schilling* [1991] based on buoyancy flux arguments. Considering our upper (75°C) and lower (25°C) estimates for the temperature anomaly at point P, the average gradient from the hot spot to the ridge axis (H to P, Figure 6) is 0.74-1.03°C/km. In contrast, the along-axis gradient is only 0.04-0.11°C/km. Therefore any successful models of sublithospheric plume dispersion must yield an along-axis temperature gradient that is an order of magnitude less than that from the hot spot to the ridge axis. Rigorous investigation of this question requires further experimental [*Kincaid*, 1994] and numerical [*Rowley et al.*, 1992] work.

Paleoaxial Temperature Anomalies

To better constrain the temporal evolution of the Galápagos ridge-hot spot system, we next examine MBA and bathymetry anomalies along paleoaxes of the Galápagos spreading center. From our model calculations we derive empirical relations between ΔT and MBA and bathymetry that we then use to estimate past temperature anomalies from the observed amplitudes of along-isochron MBA and bathymetry anomalies. In order to apply relationships derived from the active spreading center to off-axis anomalies, we must make two assumptions. First, we assume that any off-axis crustal accretion on the Cocos Plate is insignificant and that the spreading rate has not changed significantly over the past 7.7 m.y. Second, we assume the

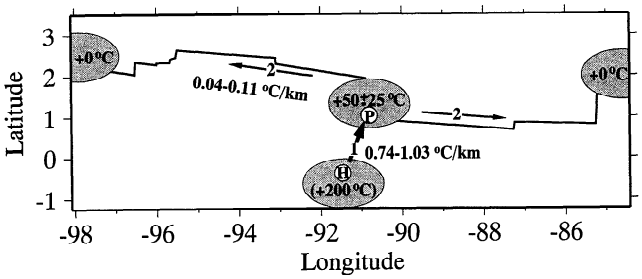

Figure 6. Map of the Galápagos region marked with estimated base layer temperature anomalies at various points along the ridge axis (solid line) and at the hot spot center (point H). Arrows point in the direction of decreasing temperature anomalies from the hot spot to ridge-axis (arrow 1) and along the ridge axis (arrows 2). Estimated temperature gradients in both directions are labeled. Note that gradient 1 is 10-20 times greater than gradient 2.

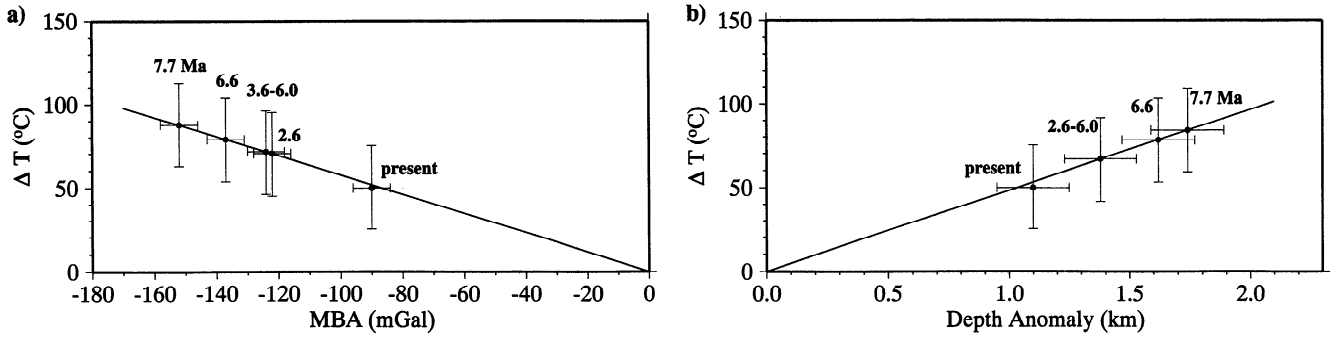

Figure 7. The empirical relationships between base layer temperature anomaly and (a) MBA and (b) bathymetry anomaly (solid lines). Also plotted are derived ΔT values for maximums in observed MBA and bathymetry along crustal isochrons (dots). Errors in gravity (12 mGal) and bathymetry (0.3) are the estimated variations due to ridge segmentation, while errors in ΔT are ±25°C, as defined according model A results.

observed MBA and bathymetry along isochrons are due primarily to the crustal structure that was frozen into the lithosphere at the time of accretion.

Our linear melting function yields an essentially linear relation between ΔT and MBA and bathymetry. This relation is derived empirically by a least squares fit between theoretical values of MBA and bathymetry and corresponding values of base layer ΔT for model A calculations. Only points further than ~80 km from transform offsets are used in the fit. The dependence of ΔT on MBA is found to be

$$\Delta T=-0.576\Delta\text{MBA} \quad (4)$$

with a < 3°C standard deviation misfit to model calculations. The dependence of ΔT on depth anomaly ΔH is found to be

$$\Delta T=48.3\Delta H \quad (5)$$

with a < 5°C standard deviation misfit to model calculations.

Using the peak mantle Bouguer and bathymetry anomalies along each isochron, we derive peak temperature anomalies beneath paleospreading centers (Figure 7). Along the 7.7 Ma isochron the observed MBA is ~150 mGal, and bathymetry

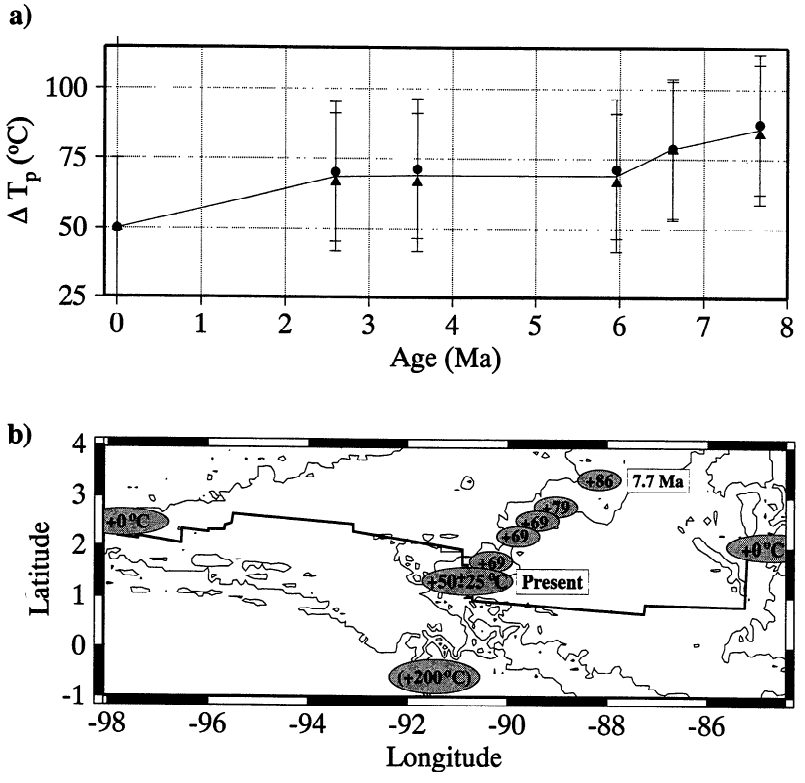

Figure 8. (a) Peak base layer ΔT calculated from MBA (circles) and bathymetry anomalies (triangles) along selected isochrons are plotted against the isochron ages. The solid line marks ΔT averaged between the gravity and bathymetry calculations. The uncertainty of ±25°C in ΔT is the uncertainty estimated from results for the present-day ridge axis. (b) Map showing the Galápagos hot spot and the locations of peak temperature anomalies along the present and paleoaxes of the Galápagos spreading center. The 3.0-, 2.0-, and 1.0-km depth intervals are contoured, and the ridge axis is marked as a bold solid line.

anomaly is ~1.7 km; these anomalies yield a past temperature anomaly of ~86±25°C, 70% greater than the anomaly along the present-day ridge axis. As shown in Figure 8a both MBA (circles) and bathymetry (triangles) relationships produce consistent temperature anomalies.

Also illustrated in Figure 8a is the decrease in amplitudes of the MBA and bathymetry anomalies with decreasing isochron age. This behavior indicates that the peak temperature anomaly beneath the Galápagos spreading center has steadily decreased since 7.7 Ma, when the hot spot was at or near the ridge axis. As the hot spot migrated southwest away from the ridge axis beneath the Nazca Plate, the maximum in ΔT decreased and the axial position of the peak in ΔT moved westward at approximately the same rate as the westward velocity component of the hot spot with respect to the Cocos Plate (Figure 8b). If we assume that the temperature anomaly of the hot spot has remained constant over the past ~8 m.y., the above results provide evidence that the amplitude of temperature anomaly beneath the Galápagos ridge axis is a function of the distance separating the hot spot and ridge axis. Such a dependence may reflect the cooling of plume material as it migrates from the Galápagos hot spot to the ridge axis and may provide importance constraints on the mechanisms of heat transfer between hot spots and nearby ridges.

Conclusions

The 2-D pattern of the mantle Bouguer and bathymetry anomalies reflect temperature-dependent density structure imposed by the Galápagos hot spot. Correlation of MBA and bathymetry with geochemical anomalies supports the notion of mixing of a hot, enriched plume with the cooler, depleted upper mantle. Profiles of mantle Bouguer gravity anomalies taken along isochrons of ages 0.0-7.67 Ma indicate that long-wavelength topography is isostatically compensated by density structure in the crust and upper 100 km of the mantle. To account for the ~90 mGal along-axis decrease in MBA and the ~1.1 km decrease in depth, our models require a subaxial temperature anomaly of 50±25°C and an associated crustal thickness increase of 3±1 km. Mantle temperatures decrease dramatically from the hot spot to the ridge axis but decrease much more gradually along axis with a lateral temperature gradient 10-20 times less. This contrast places important constraints on hot spot-to-ridge and along-ridge heat transport.

From the crustal isochron of age 7.7 Ma to the present-day axis, the along-isochron amplitudes of MBA decrease from ~150 to ~90 mGal. The corresponding along-isochron bathymetry anomalies decrease from ~1.7 to ~1.1 km. These MBA and bathymetry anomalies indicate that the axial temperature anomaly was 70% hotter in the past (86±25°C) and has steadily decreased to 50±25°C as the ridge axis migrated away from the Galápagos hot spot. The simplest explanation for this apparent decrease in the mantle anomaly beneath the Galápagos spreading center since 7.7 Ma is that the ridge axis temperature structure depends on the distance separating the hot spot and ridge axis. These conclusions point to the need for further experimental and numerical investigations to better understand the dynamic interaction between the Galápagos spreading center and hot spot and the effects of such interactive processes on the internal structure of the oceanic lithosphere.

Acknowledgments. This project was inspired by discussions with Marty Kleinrock, who also assisted in locating the Galápagos ridge-axis coordinates. We are grateful for helpful discussions with Robert Detrick, Stan Hart, and Marcia McNutt and for reviews by Gregory Neumann, John Madsen, Jean-Guy Schilling, and Norm Sleep. Douglas Wilson supplied the Cocos Plate isochron coordinates; Jason Phipps Morgan supplied the high-density gravity and bathymetry data near 95.5°W; and Marcia McNutt assisted with funding. This work was supported by NSF grants OCE9020408 and OCE9302915 and ONR grant N00014-91-J-1433.

References

Anderson, R. N., D. McKenzie, and J. G. Sclater, Gravity, bathymetry and convection in the Earth, *Earth Planet. Sci. Lett.*, *18*, 391-407, 1973.

Bell, R.E., and W.R. Buck, Crustal control of ridge segmentation inferred from observations of the Reykjanes Ridge, *Nature, 357*, 583-586, 1992.

Blackman, D. K., and D. W. Forsyth, Isostatic compensation of tectonic features of the Mid-Atlantic Ridge: 25-27°30'S, *J. Geophys. Res., 96*, 11,741-11,758, 1991.

Bonatti, E., Not so hot "hot spots" in the oceanic mantle, *Science*, 250, 107-251, 1990.

Chen, Y. J., Oceanic crustal thickness versus spreading rate, *Geophys. Res. Lett., 19*, 753-756, 1992.

Chen, Y., and W. J. Morgan, Rift valley/no rift valley transition at mid-ocean ridges, *J. Geophys. Res., 95*, 17,571-17581, 1990.

Cochran, J. R., and M. Talwani, Free-air gravity anomalies in the world's oceans and their relationship to residual elevation, *Geophys. J. R. Astron. Soc., 50*, 495-552, 1977.

Cordery, M. J., and J. Phipps Morgan, Convection and melting at mid-ocean ridges, *J. Geophys. Res., 98*, 19,477-19,503, 1993.

Crough, S. T., Thermal origin of mid-plate hot-spot swells, *Geophys. J. R. Astron. Soc., 55*, 451-469, 1978.

Crough, S. T., Hotspot swells, *Annu. Rev. Earth Planet. Sci., 11,* 165-193, 1983.

DeMets, C., R. G. Gordon, D. F. Argus, and S. Stein, Current plate motions, *Geophys. J. Int., 101*, 425-478, 1990.

Detrick, R. S., H. D. Needham, and V. Renard, Gravity anomalies and crustal thickness variations along the Mid-Atlantic Ridge between 33°N and 40°N, *J. Geophys. Res.*, in press, 1995.

Epp, D., Possible perturbations to hotspot traces and implications for the origin and structure of the Line Islands, *J. Geophys. Res., 89*, 11,273-11,286, 1984.

Feighner, M.A., and M. A. Richards, Lithospheric structure and compensation mechanisms of the Galápagos Archipelago, *J. Geophys. Res., 99*, 6711-6729, 1994.

Forsyth, D. W., Seismological constraints on partial melting beneath the East Pacific Rise (abstract), *Eos Trans. AGU, 73* (14), Spring Meeting suppl., 290, 1992.

Hart, S. R., J.-G. Schilling, and J. L. Powell, Basalts from Iceland and along the Reykjanes Ridge: Sr isotope geochemistry, *Nature Phys. Sci., 246*, 104-107, 1973.

Hey, R., Tectonic evolution of the Cocos-Nazca spreading center, *Geol. Soc. Am. Bull., 88*, 1404-1420, 1977.

Jha, K., E. M. Parmentier, and J. Phipps Morgan, The role of mantle-depletion and melt-retention buoyancy in spreading-center segmentation, *Earth Planet. Sci. Lett.*, 125, 221-234, 1994.

Kincaid, C., Laboratory experiments on the dynamics of plume-ridge interaction (abstract), *Eos Trans. AGU, 75* (16), Spring Meeting suppl., 336, 1994.

Kinzler, R. J., and T. L. Grove, Primary magmas of mid-ocean ridges and basalts 2. Applications, *J. Geophys. Res., 97*, 6907-6926, 1992.

Kuo, B.-Y., and D. W. Forsyth, Gravity anomalies of the ridge-transform system in the South Atlantic between 31° and 34.5°S: Upwelling centers and variations in crustal thickness, *Mar. Geophys. Res., 10*, 205-232, 1988.

Langmuir, C. H., E. M. Klein, and T. Plank, Petrological systematics of mid-ocean ridge basalts: constraints on melt generation beneath ocean ridges, in *Mantle Flow and Melt Generation at Mid-Ocean Ridges, Geophys. Monogr. Ser.*, vol. 71, edited by J. Phipps Morgan, D. K.

Blackman, and J. M. Sinton, pp. 183-280, AGU, Washington, D.C., 1992.

Lin , J., and E. M. Parmentier, Mechanisms of lithospheric extension at mid-ocean ridges, *Geophys. J., 96*, 1-22, 1989.

Lin, J., and J. Phipps Morgan, The spreading rate dependence of three-dimensional mid-ocean ridge gravity structure, *Geophys. Res. Lett., 19*, 13-16, 1992.

Lin, J., G. M. Purdy, H. Schouten, J.-C. Sempere, and C. Zervas, Evidence for focused magmatic accretion along the Mid-Atlantic Ridge, *Nature, 344*, 627-632, 1990.

Madsen, J. A., R. S. Detrick, J. C. Mutter, and P. Buhl, A two- and three-dimensional analysis of gravity anomalies associated with the East Pacific Rise at 9°N and 13°N, *J. Geophys. Res., 95*, 4967-4987, 1990.

Magdc, L., R. S. Dctrick, and the Tera Group, The crust and upper mantle contribution to the axial gravity anomaly at the southern East Pacific Rise, *J. Geophys. Res.*, in press, 1995.

McKenzie, D., The generation and compaction of partially molten rock, *J. Petrol., 25*, 713-765, 1984.

McKenzie, D., A. Watts, B. Parsons, and M. Roufosse, Planform of mantle convection beneath the Pacific Ocean, *Nature, 288*, 422-446, 1980.

McNutt, M., Temperature beneath midplate swells: The inverse problem, in *Seamounts, Islands, and Atolls, Geophys. Monogr. Ser.*, vol. 43, edited by B. Keating and R. Batiza, pp. 123-132, AGU, Washington, D.C., 1987.

McNutt, M., The origin of the Marquesas fracture zone ridge and its implications for the nature of hot spots., *Earth Planet. Sci. Lett., 91*, 381-393, 1989.

Michael, P. J., et al., Mantle control of a dynamically evolving spreading center: Mid-Atlantic Ridge 31-34°S, *Earth. Planet. Sci. Lett., 121*, 451-468, 1994.

Morgan, W. J., Rodriguez, Darwin, Amsterdam,..., A second type of hotspot island, *J. Geophys. Res., 83*, 5355-5360, 1978.

Morris, E., and R. S. Detrick, Three-dimensional analysis of gravity anomalies in the MARK area, Mid-Atlantic Ridge 23°N, *J. Geophys. Res., 96*, 4355-4366, 1991.

Neumann, G. A., and D. W. Forsyth, The paradox of the axial profile: Isostatic compensation along the axis of the Mid-Atlantic Ridge?, *J. Geophys. Res., 98*, 17,891-17,910, 1993.

Oxburgh, E. R., and E. M. Parmentier, Compositional and density stratification in the oceanic lithosphere—Causes and consequences, *J. Geol. Soc. London, 133*, 343-354, 1977.

Parker, R. L., The rapid calculation of potential anomalies, *Geophys. J. R. Astron. Soc., 31*, 447-455, 1973.

Parmentier, E. M., and J. Phipps Morgan, The spreading rate dependence of three-dimensional spreading center structure, *Nature, 348*, 325-328, 1990.

Phipps Morgan, J., and D. W. Forsyth, Three-dimensional flow and temperature perturbations due to a transform offset: Effect on oceanic crustal and upper mantle structure, *J. Geophys. Res., 93*, 2955-2966, 1988.

Phipps Morgan, J., and M. C. Kleinrock, Transform zone migration: Implications of bookshelf faulting at oceanic and Icelandic propagating rifts, *Tectonics, 10*, 920-935, 1991.

Phipps Morgan, J., E. M. Parmentier, and J. Lin, Mechanisms for the origin of mid-ocean ridge axial topography: Implications for the thermal and mechanical structure of accreting plate boundaries, *J. Geophys. Res., 92*, 12,823-12,836, 1987.

Prince, R. A., and D. W. Forsyth, A simple objective method for minimizing crossover errors in marine gravity data, *Geophysics, 49*, 1070-1083, 1984.

Prince, R. A., and D. W. Forsyth, Horizontal extent of anomalously thick crust near the Vema Fracture Zone from the three-dimensional analysis of gravity anomalies, *J. Geophys. Res., 93*, 8051-8063, 1988.

Reid, I., and H. R. Jackson, Oceanic spreading rate and crustal thickness, *Mar. Geophys. Res., 5* 165-172, 1981.

Rowley, C., C. W. Gable, and C. Kincaid, Dynamical interaction between upper mantle plumes and a spreading ridge: Three-dimensional experiments (abstract), *Eos Trans. AGU, 73* (43), Fall Meeting suppl., 582, 1992.

Schilling, J.-G., Iceland mantle plume geochemical evidence along Reykjanes Ridge, *Nature, 242*, 565-571, 1973.

Schilling, J.-G., Rare-earth variations across "normal" segments of the Reykjanes Ridge, 60°-53°N, Mid-Atlantic Ridge, 29°S, and East Pacific Rise, 2°-19°S, and evidence on the compositions of the underlying low velocity layer, *J. Geophys. Res., 80*, 1459-1473, 1975a.

Schilling, J.-G., Azores mantle blob: Rare earth evidence, *Earth Planet. Sci. Lett., 25*, 103-115, 1975b.

Schilling, J.-G., Upper mantle heterogeneities and dynamics, *Nature, 314*, 62-67, 1985.

Schilling, J.-G., Fluxes and excess temperatures of mantle plumes inferred from their interaction with migrating mid-ocean ridges, *Nature, 352*, 397-403, 1991.

Schilling, J.-G., R. N. Anderson, and P. Vogt, Rare earth, Fe and Ti variations along the Galapagos spreading centre, and their relationship to the Galapagos mantle plume, *Nature, 261*, 108-113, 1976.

Schilling, J.-G., R. Kingsley, and J. Devine, Galapagos hot spot-spreading center system, 1, Spatial petrological and geochemical variations (83W-101°W), *J. Geophys. Res., 87*, 5593-5610, 1982.

Sleep, N. H., Hotspots and mantle plumes: Some phenomenology, *J. Geophys. Res., 95*, 6715-6736, 1990.

Small, C., and S. T. Sandwell, An abrupt change in the ridge axis gravity with spreading rate, *J. Geophys. Res., 94*, 17,383-17,392, 1989.

Sparks, D. W., E. M. Parmentier, and J. Phipps Morgan, Three-dimensional mantle convection beneath a segmented spreading center: Implications for along-axis variations in crustal thickness and gravity, *J. Geophys. Res., 98*, 21,977-21,995, 1993.

Verma, S. P., and J.-G. Schilling, Galapagos hot spot-spreading center system, 2, $^{87}Sr/^{86}Sr$ and large ion lithophile element variations (85°W-101°W), *J. Geophys. Res., 87*, 10,838-10,856, 1982.

Verma, S. P., J.-G. Schilling, and D. G. Waggoner, Neodymium isotopic evidence for Galapagos hotspot-spreading centre system evolution, *Nature, 306*, 654-657, 1983.

Vink, G. E., A hotspot model for Iceland and the Voring Plateau, *J. Geophys. Res., 89*, 9949-9959, 1984.

Vogt, P. R., Plumes, subaxial pipe flow, and topography along the mid-oceanic ridge, *Earth Planet. Sci. Lett., 29*, 309-325, 1976.

White, R. S., A hot-spot model for early Tertiary volcanism in the N Atlantic, in *Early Tertiary Volcanism and the Opening of the NE Atlantic,* edited by A.C. Morton and L.M. Parson, *Spec. Publ. Geol. Soc. London, 39*, 3-13, 1988.

White, W. M., S. R. Hart, and J.-G. Schilling, Geochemistry of the Azores and the Mid-Atlantic Ridge: 29°N to 60°N, *Yearbook Carnegie Inst. Washington, 74*, 224-234, 1975.

White, W. M., J.-G. Schilling, and S. R. Hart, Evidence for the Azores mantle plume for strontium isotope geochemistry of the central north Atlantic, *Nature, 263*, 659-663, 1976.

White, W. M., A. R. McBirney, and R. A. Duncan, Petrology and geochemistry of the Galápagos Islands: Portrait of a pathological mantle plume, *J. Geophys. Res., 98*, 19,533-19,563, 1993.

Wilson, D. S., Confidence intervals for motion and deformation of the Juan de Fuca plate, *J. Geophys. Res, 98*, 16,053-16,071, 1993.

Wilson, D. S. and R. N. Hey, History of rift propagation and magnetization intensity for the Cocos-Nazca spreading center, *J. Geophys. Res.*, in press, 1995.

G. Ito and J. Lin, Department of Geology and Geophysics, Woods Hole Oceanographic Institution, Woods Hole, MA 02543 (e-mail: gito@magellan.whoi.edu; jlin@whoi.edu)

(Received December 22, 1993; revised September 20, 1994; accepted September 29, 1994.)